

Hydrodynamic synchronization in strong confinementIvan Tanasijević^{✉*} and Eric Lauga[†]*Department of Applied Mathematics and Theoretical Physics, University of Cambridge, Cambridge CB3 0WA, United Kingdom* (Received 29 June 2020; revised 7 November 2020; accepted 4 January 2021; published 12 February 2021)

Cellular appendages conferring motility, such as flagella and cilia, are known to synchronise their periodic beats. The origin of synchronization is a combination of long-range hydrodynamic interactions with physical mechanisms allowing the phases of these biological oscillators to evolve. Two of such mechanisms have been identified by previous work, the elastic compliance of the periodic orbit or oscillations driven by phase-dependent biological forcing, both of which can lead generically to stable phase locking. In order to help uncover the physical mechanism for hydrodynamic synchronization most essential overall in biology, we theoretically investigate in this paper the effect of strong confinement on the effectiveness of hydrodynamic synchronization. Following past work, we use minimal models of cilia where appendages are modeled as rigid spheres forced to move along circular trajectories near a rigid surface. Strong confinement is modeled by adding a second nearby surface, parallel to the first one, where the distance between the surfaces is much smaller than the typical distance between the cilia, which results in a qualitative change in the nature of hydrodynamic interactions. We calculate separately the impact of hydrodynamic confinement on the synchronization dynamics of the elastic compliance and the force modulation mechanisms and compare our results to the usual case with a single surface. Applying our results to the biologically relevant situation of nodal cilia, we show that force modulation is a mechanism that leads to phase-locked states under strong confinement that are very similar to those without confinement as a difference with the elastic compliance mechanism. Our results point therefore to the robustness of force modulation for synchronization, an important feature for biological dynamics that therefore suggests it could be the most essential physical mechanism overall in arrays of nodal cilia. We further examine the distinct biologically relevant situation of primary cilia and show in that case that the difference in robustness of the mechanisms is not as pronounced but still favors the force modulation.

DOI: [10.1103/PhysRevE.103.022403](https://doi.org/10.1103/PhysRevE.103.022403)**I. INTRODUCTION**

The world has long been fascinated by the effect of synchrony. Generally considered to be visually appealing, synchrony is often exploited in sports, such as rhythmic gymnastics or synchronized swimming, and in arts, such as dance and film. Scientists have also addressed synchronization, starting with the famous experiment of Huygens in the 17th century who noticed that two pendulum clocks hung on a wall of a boat synchronize over time [1]. The scientific interest in synchrony naturally grew over time with more examples observed in nature, such as the simultaneous flashing of fireflies [2] that sparked the idea of self-organization that seemed so “contrary to all natural laws” [3]. We later discovered that synchronization was essential for various functions of living organisms, for example the synchronization between the human circadian clock and the daylight cycle [4], and it is also responsible for the establishment of the left-right asymmetry in early stage embryos [5].

One aspect of synchronization that recently received a lot of interest is that applied to cell motility, in particular in the interactions between swimming appendages. The flagella of

many cells beat in synchrony [6,7], while cilia are known to deform collectively as metachronal waves [8–11], where neighboring cilia beat with fixed phase differences. On a scale of multiple microswimmers, hydrodynamic interactions can, for example, be responsible for the synchronization of nearby spermatozoa [12,13]. It was confirmed both experimentally [14–17] and via numerical simulations [11,18] that hydrodynamic interactions between appendages are sufficient to induce synchronization without the need for further chemical coordination, an idea that was initially proposed by Taylor [19]. Note that, in some unicellular organisms, synchronization is mediated by intracellular (basal) coupling [20].

Although hydrodynamic interactions often appear to be a necessary ingredient for synchronization, they of course need to be combined with other physical mechanisms allowing the phase of oscillators to change with time [21]. As a consequence, additional physical features of flagella and cilia have to be identified, which motivated a lot of theoretical and experimental work [22–26]. Numerous theoretical studies on this topic modeled cilia and flagella as flexible active filaments [11,18,22,25]. In order to help determine the exact physical process that, when combined with hydrodynamics, leads to synchrony, the community has also made use of minimal models of cilia where each individual cilium is replaced by a small rigid sphere driven along a circular orbit [27–29]. The simplicity of these sphere models not only allows for

*it279@cam.ac.uk

†e.lauga@damtp.cam.ac.uk

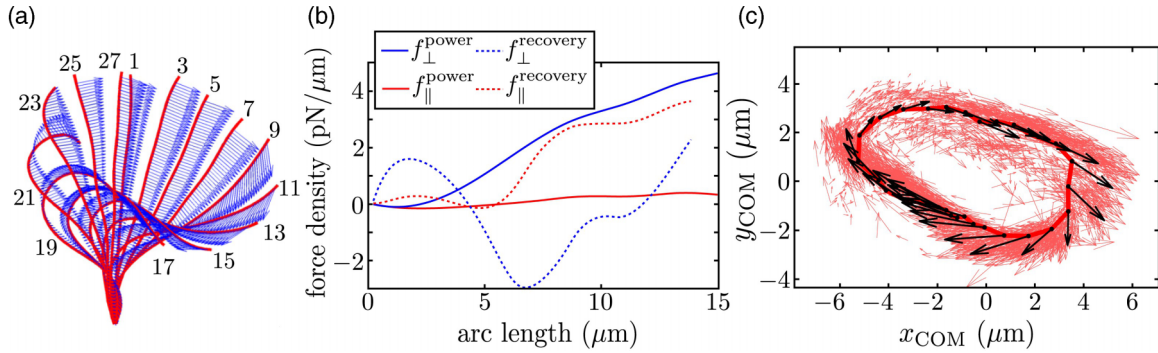


FIG. 1. Illustration of the dynamics of the ciliary beat pattern using an individual flagellum on the surface of the green alga *Volvox carteri*. (a) Example of how the shape of a flagellum or cilium evolves during a beat. (b) Force density distribution along the flagellum or cilium during the power and recovery strokes. (c) Location of the center of drag of the flagellum or cilium plotted together with the total force it exerts on the surrounding fluid. Reproduced with permission from Ref. [15], licensed under CC BY 4.0.

analytical approaches but it also makes the conclusions robust to changes in the geometrical details.

Using these minimal models, two generic physical mechanisms have been identified as enabling hydrodynamic synchronization, namely one relying on *elastic compliance* of the appendages and one requiring *modulation of the force* driving the cilia. Elastic compliance includes all features that originate from the bending elasticity of the appendage (flagellum or cilium) or of its connection to the cell. It was demonstrated to be a relevant physical mechanism leading to hydrodynamic synchronization in experiments [30], numerical simulations [31], and theoretical calculations [32]. In fact, elasticity was long thought of as a requirement to induce hydrodynamic synchronization until the force modulation mechanism was proposed in Ref. [33]. Developed specifically to address the dynamics of cilia, force modulation allows the forcing on the cilium to depend on the location of the cilium in its phase space, a model that reflects the ability of an individual cilium to undergo an asymmetric two-phase beat [9]: a power stroke vigorously pushing the fluid followed by a recovery stroke hydrodynamically hiding with a smaller disturbance to the fluid. Experiments with the flagella on the surface of the green alga *Volvox* and reproduced in Fig. 1 allow one to illustrate this asymmetric time-varying deformation and the modulation of the force experienced by the cilium along its path.

The synchronization of ciliary arrays is an important biological feature, and the lack of synchronization can lead to severe pathological conditions [34]. One way to try and distinguish between them, and potentially uncover the physical mechanism most essential overall in biology, is to probe the robustness of these mechanisms under additional constraints. Ciliary arrays are often found in confined areas of the body, such as narrow tubes or cavities inside more complex organisms. Examples include the Fallopian tube of humans [35] and the walls of the human brain ventricles [36]. Confinement is also relevant for synchronization during the close encounter of ciliated organisms with each other or with flat surfaces, e.g., collisions of two swimming *Paramecium* cells [37]. In this paper, we therefore ask the following question: What is the general impact of strong geometric confinement on the hydrodynamic synchronization of cellular appendages? We use the minimal sphere models of interacting cilia and, in

order to model the effect of strong hydrodynamic confinement, place them between two nearby parallel rigid surfaces in the limit where the distance between the surfaces is much smaller than the typical distance between the model cilia. We then investigate how each of the two synchronization mechanisms (elastic compliance vs force modulation) separately performs under confinement. We compare our results with the standard case of model cilia above a single surface and show that, in the biologically relevant situation of nodal cilia, the force modulation mechanism is significantly more robust to confinement than elastic compliance. We finally carry out a similar analysis on a second biologically motivated example, that of primary cilia; in that case, the difference in robustness between the mechanism is not as pronounced but it appears to still favor force modulation.

Our paper is organized as follows. In Sec. II, we outline the general mathematical setup and notation that is used throughout this study. In Sec. III we consider a preliminary (symmetric) example that demonstrates the differences between the mechanisms. The most general synchronization dynamics, and its comparison with the standard one-wall case, is investigated in Sec. IV with Sec. IV A devoted to the performance of elastic compliance and Sec. IV B to force modulation. In Sec. V we apply our results to the cases of nodal and primary cilia and address the robustness of the two mechanisms to confinement. We finally summarize and discuss our results in Sec. VI.

II. MODELING CILIA MOTION NEAR SURFACES

A. Minimal cilia model

One of the first mathematical models for synchronization of flagella was proposed by Taylor, who considered the interaction of a pair of two-dimensional, infinite waving sheets [19]. In order to examine analytically the collective behavior of cilia under strong confinement, it is necessary to use instead a finite-size model whose dynamics can be subject to either one of the two physical mechanisms discussed above. We thus adopt a version of the sphere model from Refs. [28,29] in which individual cilia are modeled by small rigid spheres whose motion in the fluid represents the tip of a cilium, or its center of drag, driven along a cyclic orbit.

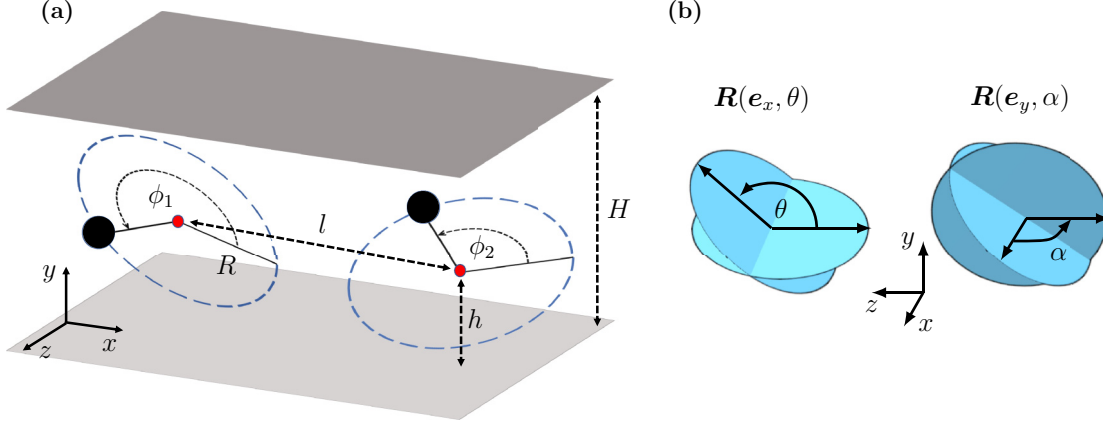


FIG. 2. Illustration of the general geometrical setup used in our minimal model of cilia dynamics near walls. (a) The relative position of the orbits and the walls. The distance between the walls H , the orbital radius R , the height of the centres above the lower wall h , the distance between the centers l , and the phase angles ϕ_1 and ϕ_2 are all clearly marked. (b) Definitions of the angles θ and α .

This minimal model is supported by experimental measurements, some of which have been reproduced in Fig. 1 in the case of the green alga *Volvox* [15]. The actual motion of an individual cilium is recorded (technically it is termed a flagellum for this organism but its dynamics is very similar to that of standard cilia) [see Fig. 1(a)]. This allows one to estimate the instantaneous velocity of the cilium along its path and, in conjunction with resistive-force theory for slender filaments [38], to predict the distribution of hydrodynamic forces along the cilium [see Fig. 1(b)]. Using the predicted force densities, a center of drag is found by weighting the arc-length positions with the corresponding force densities, and the evolution of the center of drag is shown in Fig. 1(c) together with the total drag force that the cilium exerts on the fluid. Examining the shape of its trajectory, it clearly supports the minimal model of a sphere driven along a cyclic orbit.

B. Geometry

The general situation considered in this paper is therefore a pair of such spheres, each of radius a , forced along circular orbits placed between two infinite walls that are parallel to each other; see Fig. 2. The entire gap between the walls is filled with an otherwise quiescent fluid of dynamic viscosity μ . We will also consider the case where the upper wall is not present for the purpose of comparison [32]. Unless otherwise stated the top wall is at distance H from the lower one.

The orbits, in general, will be allowed to have a variable radius R_i , $i = 1, 2$ but have a fixed center at height h from the lower wall while their centers are set a distance l apart [see notation in Fig. 2(a)]. The orientation of a particular orbit is described by two angles, θ_i (termed the tilt) and α_i in such a way that the normal to the plane of motion is $\mathbf{n}_i = \mathbf{R}(\mathbf{e}_y, \alpha_i) \cdot \mathbf{R}(\mathbf{e}_x, \theta_i) \cdot \mathbf{e}_y$ [see Fig. 2(b)], where $\mathbf{R}(\mathbf{v}, \varphi)$ is a matrix representing a rotation around the axis parallel to the vector \mathbf{v} by the angle φ in the positive mathematical sense and where \mathbf{e}_v is a unit vector in the \mathbf{v} direction. We measure the phase ϕ_i such that the radius vector of the sphere is $\mathbf{e}_{R_i} = \mathbf{R}(\mathbf{e}_y, \alpha_i) \cdot \mathbf{R}(\mathbf{e}_x, \theta_i) \cdot \mathbf{R}(\mathbf{e}_y, \phi_i) \cdot \mathbf{e}_x = \mathbf{M}_i(\phi_i) \cdot \mathbf{e}_x$. The tangential direction, in which the sphere is forced, is described by a unit vector $\mathbf{e}_{\phi_i} = -\mathbf{M}_i(\phi_i) \cdot \mathbf{e}_z$.

C. Mechanics

Following the calculations in Ref. [32] we model the elasticity of the cilium as a linear restoring force that is imposed in the radial direction and that favors the unperturbed radius R_0 . Spheres are forced along orbits by a tangential forcing $F(\phi)$, and the existence of power and recovery strokes is reflected in the explicit phase dependence of the forcing [33].

Since our goal is to model motile appendages of microorganisms, it is safe to assume that the fluid flow will be dominated by viscous forces (typically $\text{Re} \lesssim 10^{-4}$ [39]) and thus described by the incompressible Stokes equations. In the Stokes limit, the spherical spheres must be force and torque free and we can use Faxén's laws to account for the mutual interaction of the spheres to leading order [40]. The total drag on each sphere, resulting from its motion in the flow created by the neighboring sphere, is driven by the prescribed force in the tangential direction along the path and balanced by elasticity in the radial (perpendicular) direction [32,33]. At leading order in a^2/l^2 , Faxén's first law for the sphere marked with index 1 and projected onto the radial and tangential balance has the following form

$$\zeta(R_1 \dot{\phi}_1 - \mathbf{e}_{\phi_1} \cdot \mathbf{u}_{2 \rightarrow 1}) = F(\phi_1), \quad (1)$$

$$\zeta(\dot{R}_1 - \mathbf{e}_{R_1} \cdot \mathbf{u}_{2 \rightarrow 1}) = -k(R_1 - R_0), \quad (2)$$

where $\zeta = 6\pi\mu a$ is the hydrodynamic drag coefficient of the sphere, k is the spring constant of the radial elastic restoring force and $\mathbf{u}_{2 \rightarrow 1}$ is the fluid velocity of the flow caused by the motion of sphere 2 evaluated at the center of the sphere 1. Note that in a confined geometry, such as the one that we consider here, the hydrodynamic resistivity of the sphere, ζ , depends on the proximity of the sphere to either of the two walls. We will assume that the size of the sphere a is much smaller than its distance to either of the walls and thus will neglect the corrections so that ζ takes the value for a sphere in a bulk fluid.

The radial equation, Eq. (2), can then be simplified by further assuming that the elasto-hydrodynamic relaxation time, $\tau = \zeta/k$, is much shorter than the timescale on which hydrodynamic interaction changes the radius considerably.

The latter timescale increases when the interactions become weaker, i.e., when the spheres are further away from each other. Thus, we consider the far-field limit, $R \ll l$, and the quasisteady approximation outlined above can then be justified [32] by using experimental measurements of the physical parameters involved in the model [9,41]. In practical terms, this means that the term \dot{R}_1 will then be neglected in what follows, an assumption that can then be verified *a posteriori*.

D. Hydrodynamic interactions

In order to model the flow induced by each of the spheres, we use the far-field approximation, thus assuming that the spheres are much further apart than their size, $a \ll l$. Having in mind the linearity of Stokes equations we can always write the flow field as $\mathbf{u}_{2 \rightarrow 1} = \mathbf{G}(\mathbf{r}_1, \mathbf{r}_2) \cdot \mathbf{F}_2$, where \mathbf{F}_2 is the total external force applied to sphere number 2 and \mathbf{G} is a second-rank tensor. Since the restoring elastic force is a response to mutual interaction of the spheres, to leading order in a/l we have $\mathbf{F}_2 \approx F(\phi_2)\mathbf{e}_{\phi_2}$. The flow caused by a moving sphere is forced by the surface stress distribution on the surface of the sphere through the boundary integral formula. In the far-field, we then asymptotically expand the surface integral in powers of the spatial decay of the flow. The leading-order term is a point force singularity resulting from the total external force applied on the sphere. In an unbounded fluid, \mathbf{G} is a stokeslet, which has the form of the Oseen tensor $(\mathbb{I} + \mathbf{r}\mathbf{r}/r^2)/8\pi\mu r$, with $\mathbf{r} = \mathbf{r}_1 - \mathbf{r}_2$ where \mathbb{I} is the identity tensor.

Under confinement, the solid surfaces will screen hydrodynamic interactions. A standard way of dealing with hydrodynamic singularities near solid boundaries is to use image systems, similar to the one in electrostatics, where a set of hydrodynamic singularities is introduced in a fictional fluid domain within the solid boundary to balance the original singularity within the fluid and enforce the no-slip boundary condition for the flow on the surface. Classically, it was shown by Blake [42] that a stokeslet near a wall induces a set of three images, a “stokeslet equal in magnitude but opposite in sign to the initial stokeslet, a stokes-doublet and a source-doublet, the displacement axes for the doublets being in the original direction of the force.”

Adding a second wall significantly complicates the image system, and now an infinite series of hydrodynamic images with respect to each of the walls is required in order to enforce the no-slip boundary condition on both surfaces. Liron and Mochon [43] managed to simplify the expression for the leading-order flow field far from the stokeslet in the direction parallel to the surfaces, and obtained

$$\mathbf{u}_{1 \rightarrow 2} \approx \frac{3H}{2\pi\mu l^2} \left(\frac{l}{\rho}\right)^2 \underbrace{\frac{y_1}{H} \left(1 - \frac{y_1}{H}\right) \frac{y_2}{H} \left(1 - \frac{y_2}{H}\right)}_{\langle y_1, y_2 \rangle} \times \underbrace{(\mathbf{2}\hat{\rho}\hat{\rho} - \mathbb{I} + \mathbf{e}_y\mathbf{e}_y)}_{\mathbf{S}} \cdot F(\phi_1)\mathbf{e}_{\phi_1}, \quad (3)$$

where $\hat{\rho} = (\mathbb{I} - \mathbf{e}_y\mathbf{e}_y) \cdot \mathbf{r}_{1 \rightarrow 2} = l\mathbf{e}_x + O(R \cos \theta/l)$ is the relative horizontal position of the two spheres and $y_i = h + R_i \sin \theta_i \sin \phi_i$ is the y coordinate of the i th sphere. Note that we have defined the function $\langle y_1, y_2 \rangle$ in Eq. (3) as well as the tensor \mathbf{S} . This far-field flow is exact up to corrections

that decay exponentially with the horizontal distance over the characteristic length scale of the interwall distance, H . Thus, the Green’s function for hydrodynamic interactions in this setting can be well approximated by

$$\mathbf{G}(\mathbf{r}_2, \mathbf{r}_1) \approx \zeta^{-1} \beta \langle y_1, y_2 \rangle l^2 \rho^{-2} \mathbf{S}, \quad (4)$$

where $\beta \triangleq 9Ha/l^2$ is a dimensionless group that quantifies the strength of the flow due to sphere 1 near sphere 2 (or vice versa) compared with the unperturbed linear velocity of the spheres. To simplify the notation, let us introduce the tensor $\mathbf{T} \triangleq \zeta \beta^{-1} \mathbf{M}_2^T \cdot \mathbf{G} \cdot \mathbf{M}_1$, which is purely geometric and quantifies the interaction as

$$\mathbf{e}_{R_2} \cdot \mathbf{u}_{1 \rightarrow 2} \approx \beta \mathbf{e}_x \cdot \mathbf{M}_2^T \cdot \mathbf{G} \cdot (-\mathbf{M}_1) \cdot \mathbf{e}_z V_1 = -\beta T_{xz} V_1, \quad (5)$$

and similarly

$$\begin{aligned} \mathbf{e}_{\phi_2} \cdot \mathbf{u}_{1 \rightarrow 2} &\approx \beta T_{zz} V_1, \\ \mathbf{e}_{R_1} \cdot \mathbf{u}_{2 \rightarrow 1} &\approx -\beta T_{xz}^T V_2 = -\beta T_{zx} V_2, \\ \mathbf{e}_{\phi_1} \cdot \mathbf{u}_{2 \rightarrow 1} &\approx \beta T_{zz}^T V_2, \end{aligned} \quad (6)$$

where $V_i = F(\phi_i)/\zeta$ is the leading-order approximation of the instantaneous, phase-dependent, tangential velocity of the i th sphere.

E. Phase dynamics

In the asymptotic limit where the spheres are far apart, i.e., $\beta \ll 1$, and under the aforementioned assumption that the radial dynamics are quasisteady, the radial equation (2) for the first sphere yields $R_1 = R_0 - \beta \tau T_{zx} V_2$. Substituting R_1 into the phase equation, Eq. (1), we obtain

$$\dot{\phi}_1 = (V_1 + \beta T_{zz} V_2) R_0^{-1} \left(1 - \beta \tau T_{zx} \frac{V_2}{R_0}\right)^{-1}. \quad (7)$$

After expanding the right-hand side of Eq. (7) to first order in β and carrying out the same procedure for the second sphere, the phase evolution ends up being described by the coupled system of nonlinear equations

$$\dot{\phi}_1 = \frac{F(\phi_1)}{\zeta R_0} + \beta \frac{F(\phi_2)}{\zeta R_0} T_{zz} + \beta \tau \frac{F(\phi_1) F(\phi_2)}{\zeta R_0 \zeta R_0} T_{zx}, \quad (8)$$

$$\dot{\phi}_2 = \frac{F(\phi_2)}{\zeta R_0} + \beta \frac{F(\phi_1)}{\zeta R_0} T_{zz} + \beta \tau \frac{F(\phi_2) F(\phi_1)}{\zeta R_0 \zeta R_0} T_{zx}. \quad (9)$$

For most of the calculations presented here it will be necessary to simplify the tensor \mathbf{T} by truncating it at leading order in R/l , and, under this approximation, \mathbf{S} simplifies to $\mathbf{e}_x\mathbf{e}_x - \mathbf{e}_z\mathbf{e}_z$.

In order to examine solely the effects of elastic compliance, we set $F(\phi) = \zeta R_0 \omega_0$ to be constant, where ω_0 is the angular frequency of an isolated sphere. In contrast, in order to examine solely the effects of force modulation, we set $k \rightarrow \infty$ (which implies $\tau = 0$).

F. Synchronization

Two oscillators are said to synchronize if, through mutual interaction, the phase difference $\phi_2 - \phi_1$ converges to a value that is constant in time (a phase-locked state). However, when the forcing is phase dependent, the measured phase difference can be dominated by the difference in forcing and the final synchronization states (other than completely in phase)

are less physically obvious from the information on $\phi_2 - \phi_1$. A way of solving this problem, without having to compare the contributions from the phase dependent forcing and the interactions, is to change below to a different phase gauge so that the phase-dependent forcing effects are essentially factored out. Note that this new phase gauge is, in fact, how the phase is often defined in literature for complex systems with periodic dynamics [44]; due to the physical meaning of the geometric phase ϕ introduced above, we choose to refer to it as a different phase gauge. Namely, it is denoted by $\Phi(\phi)$ and defined as

$$\Phi(\phi) = 2\pi \frac{K(\phi)}{K(2\pi)}, \quad \text{where } K(\phi) = \int_0^\phi \frac{d\phi'}{F(\phi')}, \quad (10)$$

which evolves in time at a constant rate for an isolated sphere. Indeed, $\Phi(0) = 0$, $\Phi(2\pi) = 2\pi$, so Φ changes by 2π during a single revolution of the bead and, for an isolated sphere, we have

$$\dot{\Phi} = \frac{2\pi}{K(2\pi)} \frac{\dot{\phi}}{F(\phi)} = \frac{2\pi}{K(2\pi)} (\zeta R_0)^{-1} \triangleq \Omega = \text{const.} \quad (11)$$

Hence, this transformation is a proper change of phase gauge and, for two spheres with the same orbit properties, the phase difference in the new gauge will depend only on the interactions. In situations where the force modulation model is examined, we will be interested in the time evolution of $\Delta \triangleq \Phi_1 - \Phi_2$. As we will usually be interested in the case where the force modulation is weak, i.e., the forcing varies only weakly from its mean value, the difference $\Phi(\phi) - \phi$ will be small, on the order of force modulation. Thus, if we reach a phase locked state $\Delta \equiv \Delta_0$ in the new gauge, we could say that $\phi_1 - \phi_2 \sim \Delta_0$, asymptotically, with corrections on the order of the force modulation. As long as Δ_0 is of order $O(1)$ this is an asymptotically correct statement, which will allow us to conclude on the physics of synchronization. However, $\Phi_1 - \Phi_2 \equiv 0$ implies $\phi_1 - \phi_2 \equiv 0$, so the asymptotic expression fails only for small but nonzero Δ_0 , and this should be kept in mind when deriving physical conclusions.

III. CILIA ORBITS IN THE MIDPLANE

In this section, we first consider the case where the spheres are orbiting in the plane located exactly halfway between the two walls and parallel to both. This simple setup allows us to illustrate two important points: (i) the presence of the second (upper) wall has a markedly different impact on the elastic compliance and force modulation mechanisms, and (ii) the relative orientation of the cilia is an important factor in both cases. Although the situation where the orbits are parallel to the walls is not a perfect representation of ciliary beats, for any periodically forced quasi-two-dimensional structure tightly fitting between plates, e.g., active artificial microgels [45], this is a relevant limit to consider.

Setting the orbits in the midplane with $\alpha_i = \theta_i = 0$ leads to a couple of mathematical simplifications. In that case, $\langle y_1, y_2 \rangle$ is exactly equal to $1/16$ so we will absorb it into $\beta = 9Ha/16l^2$, only in this section; furthermore, \mathbf{T} turns out to be a symmetric tensor even without approximating the interaction kernel \mathbf{S} . Knowing that $T_{xz} = T_{zx}$ makes it then obvious that a completely in-phase state $\phi_1 = \phi_2$ is a solution

of Eqs. (8) and (9), but to say the spheres synchronize in-phase we have to investigate the stability of this state.

A. No synchronization by elastic compliance

First we address the case where the forcing along the orbit is constant, i.e., the elastic compliance model. Considering both Eqs. (8) and (9), with the terms $F(\phi_i)/\zeta R_0$ replaced by ω_0 , and since \mathbf{T} is symmetric even without the linearization of the interaction kernel in $R_0/l \ll 1$, the phase difference $\phi_1 - \phi_2$ remains constant up to $O(\beta^2)$. This means that the elastic compliance mechanism leads to no synchronization up to order $O(\beta^2)$. Comparing to the case of cilia orbits near a single wall [32], where the spheres always synchronize to an in-phase state at leading order in β , we thus see that in the presence of strong hydrodynamic confinement disables elastic compliance as a synchronization mechanism.

B. Synchronization by force modulation

In the force modulation model (i.e., in the limit $\tau \rightarrow 0$), we can examine the linear stability of the in-phase state ϕ by introducing a small perturbation in the form $\phi_1 = \phi + \Delta$, $\phi_2 = \phi$, where

$$\dot{\phi} = \frac{F(\phi)}{\zeta R_0} [1 + \beta T_{zz}(\phi, \phi)]. \quad (12)$$

By calculating the average of the perturbation growth rate, $\langle \sigma \rangle$, and examining its sign over a single beat it is then possible to conclude on the stability characteristics of the in-phase state. The linearization of Eqs. (8) and (9) for small Δ leads to

$$\begin{aligned} \dot{\Delta} &= \frac{F(\phi + \Delta) - F(\phi)}{\zeta R_0} [1 - \beta T_{zz}(\phi + \Delta, \phi)] \\ &= \frac{F'(\phi)}{\zeta R_0} [1 - \beta T_{zz}(\phi, \phi)] \Delta + O(\Delta^2), \end{aligned} \quad (13)$$

which allows us to calculate the time-averaged growth rate as

$$\begin{aligned} \langle \sigma \rangle &\equiv \frac{1}{T_0} \int_t^{t+T_0} \frac{\dot{\Delta}}{\Delta} dt = \frac{1}{T_0} \int_0^{2\pi} \frac{F'(\phi)}{F(\phi)} \frac{1 - \beta T_{zz}}{1 + \beta T_{zz}} d\phi \\ &= -\frac{2\beta}{T_0} \int_0^{2\pi} \frac{F'(\phi)}{F(\phi)} T_{zz} d\phi + O(\beta^2), \end{aligned} \quad (14)$$

where T_0 is the period of the in-phase state ϕ . These results turn out to be identical to those obtained in the case of a single wall [33] since both are characterized by $T_{zz}(\phi, \phi) = -C \cos 2\phi + \text{const}$, with $C > 0$. A particular forcing function $F(\phi)$ that leads to in-phase synchronization near a single wall will do so in the presence of the second one and vice versa, at order β . Thus, in this setting, the force modulation mechanism is robust to strong hydrodynamic confinement.

C. Impact of the relative orientation

To illustrate the importance of the relative orientation of the orbits in this situation, we can consider the situation where one of them has been flipped by 180° , i.e., we let $\theta_2 = \pi$. Physically this models a situation where the cilia are tethered on the opposing walls and thus they beat in different directions.

In this case, the tensor \mathbf{T} is no longer symmetric and the subtraction of Eqs. (8) and (9) under the elastic compliance model [$F(\phi) = \zeta R_0 \omega_0$] yields the equation for the phase difference $\Delta = \phi_1 - \phi_2$ as

$$\dot{\Delta} \approx -2\beta\tau\omega_0^2 \sin \Delta, \quad (15)$$

with corrections of order R/l . This is the famous Adler equation with a stable equilibrium at $\Delta \equiv 0$, and cilia always synchronize to a completely in-phase state in that case. If the case above of spheres beating in the same direction has indicated that elastic compliance might lead to no synchronization in strong confinement, this shows that the relative orientation is an important factor that needs to be carefully included in any further investigation.

Beyond two-cilia synchronization, elastic compliance can also lead to the development of metachronal waves for cilia beating in alternating directions. Consider a linear array of $2N$ model cilia, each at a distance l from its neighbors and orbiting in the midplane such that $\theta_{2k} = 0$ and $\theta_{2k-1} = \pi$ for $k = 1, \dots, N$. We assume that each sphere interacts only with its nearest neighbors on either side. Assuming periodic boundary conditions where the spheres at the ends of the array interact with each other, the evolution equation becomes

$$\begin{aligned} \dot{\phi}_n &= \omega_0 + \beta\omega_0(\cos \chi_n + \cos \chi_{n+1}) \\ &\quad + \beta\tau\omega_0^2(\sin \chi_{n+1} - \sin \chi_n), \end{aligned} \quad (16)$$

$$\begin{aligned} \dot{\chi}_n &= \beta\omega_0(\cos \chi_{n+1} - \cos \chi_{n-1}) + \beta\tau\omega_0^2(\sin \chi_{n+1} \\ &\quad - 2 \sin \chi_n + \sin \chi_{n-1}), \end{aligned} \quad (17)$$

where $\chi_n = \phi_n - \phi_{n-1}$. The same set of equations was reported in Ref. [32] for a chain of oscillators beating in the same direction near a single wall. Clearly, the system in Eq. (17) admits a solution $\chi_n = \Phi = \text{const}$, which corresponds to a metachronal wave where the neighboring oscillators beat at the constant phase difference Φ . This wave is unstable for $\cos \Phi < 0$ and marginally stable for $\cos \Phi \geq 0$. We have verified the existence of these metachronal waves numerically for an array of 50 spheres with periodic boundary conditions and starting from random initial phases. Our results are illustrated numerically in Fig 3 in the form of the time evolution of the phases ϕ_n [Fig. 3(a)] and the phase differences of the neighboring spheres χ_n [Fig. 3(b)]. More precisely, $[(\chi_n - \pi) \bmod 2\pi]/\pi$ is plotted as a proxy for χ_n . Over time, the system reaches a metachronal state with χ_n close to 0 for all $n = 1, \dots, 50$, which agrees with the prediction that the waves with $\cos \chi_n \geq 0$ are marginally stable.

This setup is the simplest possible one to investigate the organization of many cilia and it shows that the mechanism is able to produce the same phenomenon (metachronal waves) as in the single-wall case [32]. Including full long-range interactions beyond the nearest-neighbor case might further change the global organization of cilia. It was previously shown that a similar minimal model exhibits near a single surface a transition from metachronal waves to more complex states as the range of the interactions increases [46]. The different nature of the Green's function in strong confinement, including the presence of the additional length scale H , could of course lead to different dynamics than in the single wall case.

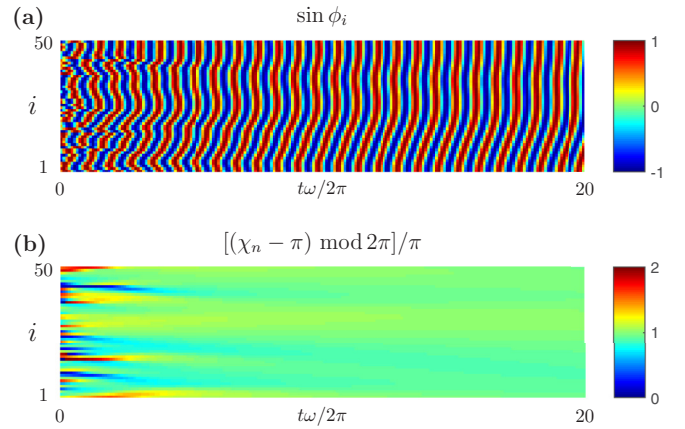


FIG. 3. Formation of metachronal waves from random initial conditions with periodic boundary conditions for an array of cilia beating in alternating directions. We plot the time evolution of $\sin \phi_i$ in subfigure (a) and $[(\chi_n - \pi) \bmod 2\pi]/\pi$ in subfigure (b) with $i = 1, \dots, N$. Simulations were done for $N = 50$ cilia with $\beta = 0.16$ and $\lambda = \tau\omega = 0.9$. Values for β and λ are chosen to be relatively large only for the purpose of reducing the number of periods the system takes for developing the metachronal waves.

IV. CILIA WITH ARBITRARILY ORIENTED ORBITS

As shown in the previous section, the orientation of the cilia orbits play a crucial role in allowing synchronization to take place. In this section, we therefore allow the orientations of the cilia arrays to be arbitrary and compute mathematically the consequence on the synchronization dynamics for both physical mechanisms. We will then apply our mathematical results to two biologically relevant cases in Sec. V.

A. Hydrodynamic synchronization by elastic compliance

In this first part, we address the synchronization by elastic compliance. We use our general derivation in Eqs. (8) and (9) and exclude the force modulation by setting $F(\phi) = \zeta R\omega_0 = \text{const}$, which results in the phase dynamics

$$\dot{\phi}_1 = \omega_0 + \beta\tau\omega_0^2 T_{zx} + \beta\omega_0 T_{zz}, \quad (18)$$

$$\dot{\phi}_2 = \omega_0 + \beta\tau\omega_0^2 T_{xz} + \beta\omega_0 T_{zz}. \quad (19)$$

By subtracting these two equations, we obtain an equation for the phase difference $\Delta = \phi_1 - \phi_2$ as

$$\dot{\Delta} = \dot{\phi}_1 - \dot{\phi}_2 = \beta\tau\omega^2(T_{zx} - T_{xz}). \quad (20)$$

We can next simplify \mathbf{T} at leading order in R_0/l by approximating $l/\rho \approx 1$ and $\hat{\rho} \approx \mathbf{e}_x$, which leads to

$$\begin{aligned} \dot{\Delta} &\approx -\beta\tau\omega^2(y_1, y_2)[(\cos \theta_1 - \cos \theta_2) \sin(\alpha_1 + \alpha_2) \cos \Delta \\ &\quad + (1 - \cos \theta_1 \cos \theta_2) \cos(\alpha_1 + \alpha_2) \sin \Delta]. \end{aligned} \quad (21)$$

The result in Eq. (21) resembles the Adler equation, a resemblance we can make more obvious using a few algebraic manipulations. Defining $r_2 \triangleq [(1 - \cos \theta_1 \cos \theta_2)^2 \cos(\alpha_1 + \alpha_2)^2 + (\cos \theta_2 - \cos \theta_1)^2 \sin(\alpha_1 + \alpha_2)^2]^{1/2} \geq 0$ and the

angle $\Delta_0^{(2)}$ as

$$r_2 \cos \Delta_0^{(2)} = (1 - \cos \theta_1 \cos \theta_2) \cos(\alpha_1 + \alpha_2), \quad (22)$$

$$r_2 \sin \Delta_0^{(2)} = (\cos \theta_2 - \cos \theta_1) \sin(\alpha_1 + \alpha_2), \quad (23)$$

transforms Eq. (21) into

$$\dot{\Delta} = -\beta \tau \omega^2 \langle y_1, y_2 \rangle r_2 \sin(\Delta - \Delta_0^{(2)}). \quad (24)$$

Note that we have used the superscript 2 in the notation $\Delta_0^{(2)}$ in order to emphasize that this is the result in the case of two walls. Since all the prefactors in Eq. (24), including r_2 and $\langle y_1, y_2 \rangle$, are positive numbers, the phase difference $\Delta_0^{(2)}$ is the linearly stable solution to Eq. (24) while $\Delta_0^{(2)} + \pi$ is the unstable solution. This is true even though the term $\langle y_1, y_2 \rangle$ is, in fact, phase dependent and therefore Eq. (24) is not entirely equivalent to the Adler's equation. It is important to note that both r_2 and $\Delta_0^{(2)}$ are a function of the orientation of the orbits only. Note that the prefactor r_2 indicates that the magnitude of the contribution of the hydrodynamic interactions to the rate of change of the phase difference strongly depends on the orientation of the orbits. It is therefore an important factor in quantifying the strength of synchronization towards $\Delta_0^{(2)}$ and thus in measuring the importance of hydrodynamic interactions relative to any other effects not included in our model, for example noise of any kind.

We can now compare these results with the case of a single wall. Past work involving solely elastic compliance as the synchronization mechanism has considered only the horizontal orbits, so for the purpose of comparison we adjust the model of Ref. [32] to arbitrarily oriented orbits close to a single wall. We obtain that result by changing the interaction kernel to a linearized Blake tensor $\tilde{\beta} \mathbf{e}_x \mathbf{e}_x$. Here, $\tilde{\beta} \triangleq 9ah^2/l^3$ and it is a parameter analogous to β but relevant to the single-wall case. These nondimensional groups are a relative measure of the speed of synchronization since the number of periods around the orbits required before reaching a synchronized state is proportional to $1/\beta$.

After performing the same calculations as for the case of two walls, we obtain

$$\begin{aligned} \dot{\Delta} &= \tilde{\beta} \tau \omega^2 (T_{xx} - T_{xz}) \\ &\approx -\tilde{\beta} \tau \omega^2 [(\cos \theta_1 \sin \alpha_1 \cos \alpha_2 - \cos \theta_2 \sin \alpha_2 \cos \alpha_1) \cos \Delta \\ &\quad + (\cos \alpha_1 \cos \alpha_2 + \sin \alpha_1 \sin \alpha_2 \cos \theta_1 \cos \theta_2) \sin \Delta], \end{aligned} \quad (25)$$

and we see synchronization similar to the case of two walls. Defining $r_1 > 0$ as

$$\begin{aligned} r_1^2 &= (\cos \theta_1 \sin \alpha_1 \cos \alpha_2 - \cos \theta_2 \sin \alpha_2 \cos \alpha_1)^2 \\ &\quad + (\cos \alpha_1 \cos \alpha_2 + \sin \alpha_1 \sin \alpha_2 \cos \theta_1 \cos \theta_2)^2, \end{aligned} \quad (26)$$

and the angle $\Delta_0^{(1)}$ via

$$r_1 \cos \Delta_0^{(1)} = \cos \alpha_1 \cos \alpha_2 + \sin \alpha_1 \sin \alpha_2 \cos \theta_1 \cos \theta_2, \quad (27)$$

$$r_1 \sin \Delta_0^{(1)} = -\cos \theta_1 \sin \alpha_1 \cos \alpha_2 + \cos \theta_2 \sin \alpha_2 \cos \alpha_1, \quad (28)$$

we obtain

$$\dot{\Delta} = -\tilde{\beta} \tau \omega^2 r_1 \sin(\Delta - \Delta_0^{(1)}). \quad (29)$$

Notice also that there is no synchronization to leading order if and only if $r_1 = 0$. It is notable that this condition can arise in the case of identical orbits $\alpha_i = \alpha_0$ and $\theta_i = \theta_0$. In this case, $r_1 = 0$ is equivalent to $\alpha_0 = \pm\pi/2$ and $\theta_0 = \pm\pi/2$, which is the case of vertical orbits perpendicular to the x axis, i.e., to the direction connecting its centres. Intuitively this is clear since we linearized the Blake tensor to $\tilde{\beta} \mathbf{e}_x \mathbf{e}_x$, so in this case orbits have no interaction to this order.

Thus, we have found that in both cases, one or two walls, the system synchronizes to a phase locked state. The value of that terminal phase difference $\Delta_0^{(i)}$ (where the label i is the number of walls in the setup) is different in cases of one and two walls and it is also a function of the orientation of the orbits. In Sec. V, we will quantify the difference between $\Delta_0^{(1)}$ and $\Delta_0^{(2)}$ in two biologically relevant cases and use this information as a measure of robustness to confinement of the elastic compliance as a mechanism for hydrodynamic synchronization.

B. Hydrodynamic synchronization by force modulation

In order to address the force modulation model, we follow the approach outlined in Sec. II F and perform a change of variable, $\Phi(\phi)$, so that the new phase variable now grows in time at constant rate $\Omega = 2\pi/T_0$, where T_0 is the oscillation period of an isolated model cilium. The change of variables is given by

$$\Phi(\phi) = 2\pi \frac{K(\phi)}{K(2\pi)}, \quad \text{where } K(\phi) = \int_0^\phi \frac{d\phi'}{F(\phi')}, \quad (30)$$

or, equivalently, $\dot{\Phi} = \dot{\phi}/F(\phi)$. If we now let $\Phi_i = \Phi(\phi_i)$ and introduce $\bar{\Phi} = \frac{1}{2}(\Phi_1 + \Phi_2)$ and $\Delta = \Phi_1 - \Phi_2$, we can anticipate that Δ is a slow variable and $\Delta = 0$ is an in-phase solution. In general, it is possible to invert Eq. (30) so that $\phi_i = \phi(\Phi_i) = \phi(\bar{\Phi} \pm \Delta/2)$ and the phase evolution equations (8) and (9) become

$$\frac{\dot{\Phi}_1}{\Omega} = 1 + \beta \frac{F(\Phi_2)}{F(\Phi_1)} T_{zz}(\Phi_1, \Phi_2), \quad (31)$$

$$\frac{\dot{\Phi}_2}{\Omega} = 1 + \beta \frac{F(\Phi_1)}{F(\Phi_2)} T_{zz}(\Phi_1, \Phi_2), \quad (32)$$

where we have used the shorthand notation $f(\bar{\Phi}) \equiv f(\phi(\bar{\Phi}))$. Subtracting these two equations leads to

$$\begin{aligned} \dot{\Delta} &= \beta \Omega \left[\frac{F(\bar{\Phi} - \Delta/2)}{F(\bar{\Phi} + \Delta/2)} - \frac{F(\bar{\Phi} + \Delta/2)}{F(\bar{\Phi} - \Delta/2)} \right] \\ &\quad \times T_{zz}(\bar{\Phi} + \Delta/2, \bar{\Phi} - \Delta/2) \\ &\equiv W(\bar{\Phi}, \Delta). \end{aligned} \quad (33)$$

Under the assumption of weak interaction $\beta \ll 1$, we confirm *a posteriori* that Δ is indeed a slow variable and $\bar{\Phi} \approx \Omega t$ at leading order in β .

In order to examine the evolution of the phase difference, it is instructive to coarse grain the timescale by averaging Eq. (33) over the fast period of the mean phase, as

$$\langle \dot{\Delta} \rangle = \frac{1}{2\pi} \int_0^{2\pi} W(\bar{\Phi}, \Delta) d\bar{\Phi} \equiv -\frac{dV(\Delta)}{dt}, \quad (34)$$

where we have defined the effective potential that governs the long-time evolution of Δ . The location of the global minimum of V , if it existed, would be the state to which the system synchronizes; the goal is therefore to determine this potential. However, since $W(\Phi, \Delta)$ is a periodic function in Δ , the function $V(\Delta)$ must have the form of a tilted washboard potential with no global minimum. A real physical system would thus spend a relatively long time in the local minima with occasional biased phase slips to the other minima caused by the stochastic noise (not included in our model). This feature has been observed in experiments [15] and is correctly captured by the force modulation model [33]. Hence, the relevant features of the potential $V(\Delta)$ for the synchronization are (i) the location of local minima inside the interval $[-\pi, \pi[$ and (ii) the direction of the tilt.

Since it is difficult to proceed further with a general force profile, we will focus the first mode of force modulation, $F(\phi) = F_0[1 + A \sin(\phi + \delta)]$. This choice is motivated by

experimental results on the dynamics of short flagella on the somatic cells of *Volvox carteri* [15]. As shown in Fig. 1, a hydrodynamic point force was fitted to measured flow field from beating cilia; the magnitude of this fitted force shows one strong peak during a single beat, suggesting that the fundamental mode of force modulation is dominant.

The assumption that $A \lesssim 1$ allows us to invert Eq. (30) up to $O(A^2)$ and obtain

$$\begin{aligned} \phi(\Phi) = & \Phi + [\cos \delta - \cos(\Phi + \delta)]A + \left\{ \sin(\Phi + \delta)[\cos \delta \right. \\ & \left. - \cos(\Phi + \delta)] + \frac{1}{4}[\sin(2\Phi + 2\delta) - \sin 2\delta] \right\} A^2 \\ & + O(A^3). \end{aligned} \quad (35)$$

Furthermore, in the process of recovering the effective potential $V(\Delta)$ the terms are truncated at $O(A^3)$ since, based on the single wall case [33], we expect synchronization at that order. We also approximate the hydrodynamic interactions at leading order in R/l so that

$$\begin{aligned} T_{zz}(\phi_1, \phi_2) \approx & \langle y_1, y_2 \rangle \{ \cos(\alpha_1 + \alpha_2)[\sin \phi_1 \sin \phi_2 - \cos \theta_1 \cos \theta_2 \cos \phi_1 \cos \phi_2] \\ & + \sin(\alpha_1 + \alpha_2)[\cos \theta_1 \cos \phi_1 \sin \phi_2 + \cos \theta_2 \cos \phi_2 \sin \phi_1] \}. \end{aligned} \quad (36)$$

The derivation of Eq. (36) is the last step in this section that can be carried out by hand, while in what follows we employ symbolic manipulation using *Mathematica*. Due to a large number of parameters of this model, even with the simplification of working to second order in A , the potential $V(\Delta)$ ends up having 5131 term and therefore we omit its full form here. We can proceed by making the further assumption

that h and R are of comparable magnitude. This is supported by experimental measurements of the cilium beating pattern [47] and by the fact that a sphere in the minimal cilium model is meant to represent the tip of a cilium [28], so both the size of the orbit and the height above the surface are expected to have the same scaling. Keeping only the leading-order terms in h/H and R/H , we then obtain

$$V(\Delta) = \beta \Omega A \frac{hR}{H^2} \left(C_0 \Delta + B_1(1 - \cos \Delta) + \frac{B_2}{2}(1 - \cos 2\Delta) + A_1 \sin \Delta + \frac{A_2}{2} \sin 2\Delta \right) + O(A^2(h/H)^2, A(h/H)^3), \quad (37)$$

where the five constants are now defined as

$$C_0 = -\frac{1}{2}[\sin 2\alpha \sin \delta \sin(\theta_1 - \theta_2) + \cos 2\alpha \cos \delta (\sin \theta_1 - \sin \theta_2)], \quad (38)$$

$$B_1 = -\frac{1}{8}\{2 \cos 2\alpha \sin \delta (\sin \theta_1 + \sin \theta_2)(\cos \theta_1 \cos \theta_2 + 1) + \sin 2\alpha \cos \delta [-6 \sin(\theta_1 + \theta_2) + \sin 2\theta_1 + \sin 2\theta_2]\}, \quad (39)$$

$$B_2 = -\frac{1}{4}\{\cos 2\alpha \sin \delta (\sin \theta_1 + \sin \theta_2)(1 - \cos \theta_1 \cos \theta_2) + \sin 2\alpha \cos \delta [1 - \cos(\theta_1 - \theta_2)] \sin(\theta_1 + \theta_2)\}, \quad (40)$$

$$A_1 = -\frac{1}{4}(\sin \theta_1 - \sin \theta_2)[\cos 2\alpha \cos \delta (\cos \theta_1 \cos \theta_2 - 3) - \sin 2\alpha \sin \delta (\cos \theta_1 + \cos \theta_2)], \quad (41)$$

$$A_2 = \frac{1}{4}\{\sin 2\alpha \sin \delta \sin(\theta_1 - \theta_2)[1 - \cos(\theta_1 + \theta_2)] + \cos 2\alpha \cos \delta (\sin \theta_1 - \sin \theta_2)(\cos \theta_1 \cos \theta_2 - 1)\}, \quad (42)$$

and $2\alpha = \alpha_1 + \alpha_2$. In Fig. 4, we plot the full potential $V(\Delta)$ and its leading-order approximation, Eq. (37), for $A = 0.1$ and $R = h = 0.1H$ (top row). Note that since our focus is on the landscape, and specifically the location of the local minima, we do not need to include the prefactors when plotting the leading order in Fig. 4, right. Even for the relatively large values of the parameters treated as small in the calculations, we see that the landscape of the leading-order approximation agrees well with the full expression.

For the purposes of comparison, we can then repeat the calculations in the case of a single wall; to best of our knowledge,

the effective potential arising for arbitrarily oriented orbits has not been reported in the literature, though the potentials were previously calculated and plotted for a few cases with $\theta_1 = \theta_2$ in [48]. The only adjustment necessary in the calculations consists in altering the interaction kernel, where we now use the Blake tensor linearized in R/l , $\zeta^{-1} \tilde{\beta} h^{-2} y_1 y_2 \mathbf{e}_x \mathbf{e}_x$. Assuming again that the radii of the orbits and their distances to the substrate are comparable, we obtain in the one-wall case

$$\begin{aligned} T_{zz} = & \frac{y_1 y_2}{h^2} (\cos \phi_1 \cos \theta_1 \sin \alpha_1 + \cos \alpha_1 \sin \phi_1) \\ & \times (\cos \phi_2 \cos \theta_2 \sin \alpha_2 + \cos \alpha_2 \sin \phi_2), \end{aligned} \quad (43)$$

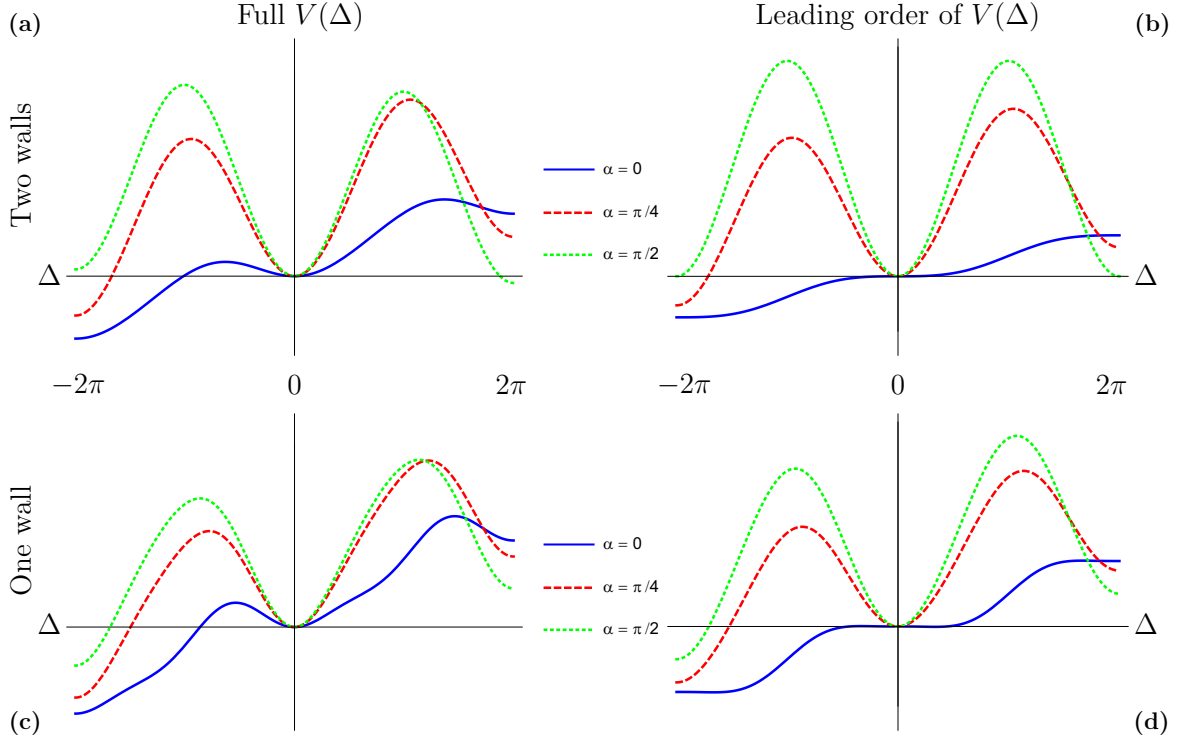


FIG. 4. Effective synchronization potential $V(\Delta)$ for three different values of $\alpha = (\alpha_1 + \alpha_2)/2 = 0, \pi/4, \pi/2$. Top row: Two-wall case, full potential $V(\Delta)$ [in (a)] and its leading-order approximation in h/H and R/H [in (b)] for $\theta_1 = 0.4, \theta_2 = 0.45, A = 0.1, R = h = 0.1H$, and $\delta = 0$. Bottom row: Analogous potentials for the single-wall case [(c) and (d), corresponding to (a) and (b), respectively]. Note the vertical axes are scaled differently, which does not affect the location of the local minima in each graph.

with $\tilde{\beta} = 9ah^2/l^3$, which is the same as previously defined in elastic compliance subsection. Finally, the potential ends up having the exact same form as Eq. (37) in the case of two walls but with a different prefactor of $\tilde{\beta}\Omega AR/h$ and with the constants now defined as

$$C_0 = \frac{1}{2}[\cos \alpha_2 \sin \theta_2 (\sin \alpha_1 \sin \delta \cos \theta_1 + \cos \alpha_1 \cos \delta) - \cos \alpha_1 \sin \theta_1 (\sin \alpha_2 \sin \delta \cos \theta_2 + \cos \alpha_2 \cos \delta)], \quad (44)$$

$$B_1 = \frac{1}{4}\{\sin \alpha_2 \cos \theta_2 [\cos \alpha_1 \cos \delta (3 \sin \theta_1 - \sin \theta_2) + \sin \alpha_1 \sin \delta \cos \theta_1 (\sin \theta_1 + \sin \theta_2)] - \cos \alpha_2 [\sin \alpha_1 \cos \delta \cos \theta_1 (\sin \theta_1 - 3 \sin \theta_2) + \cos \alpha_1 \sin \delta (\sin \theta_1 + \sin \theta_2)]\}, \quad (45)$$

$$B_2 = \frac{1}{4}\{\cos \alpha_2 [\sin \alpha_1 \cos \delta \cos \theta_1 (\sin \theta_1 - \sin \theta_2) - \cos \alpha_1 \sin \delta (\sin \theta_1 + \sin \theta_2)] - \sin \alpha_2 \cos \theta_2 [\cos \alpha_1 \cos \delta (\sin \theta_1 - \sin \theta_2) + \sin \alpha_1 \sin \delta \cos \theta_1 (\sin \theta_1 + \sin \theta_2)]\}, \quad (46)$$

$$A_1 = \frac{1}{4}(\sin \theta_1 - \sin \theta_2)[\sin \alpha_1 \cos \theta_1 (\sin \alpha_2 \cos \delta \cos \theta_2 + \cos \alpha_2 \sin \delta) + \cos \alpha_1 (\sin \alpha_2 \sin \delta \cos \theta_2 + 3 \cos \alpha_2 \cos \delta)], \quad (47)$$

$$A_2 = \frac{1}{4}\{\cos \alpha_1 [\cos \alpha_2 \cos \delta (\sin \theta_2 - \sin \theta_1) + \sin \alpha_2 \sin \delta \cos \theta_2 (\sin \theta_1 + \sin \theta_2)] - \sin \alpha_1 \cos \theta_1 [\sin \alpha_2 \cos \delta \cos \theta_2 (\sin \theta_1 - \sin \theta_2) + \cos \alpha_2 \sin \delta (\sin \theta_1 + \sin \theta_2)]\}. \quad (48)$$

Similarly to the case of two walls, this leading-order approximation in h/H and R/H agrees well with the full form for relatively large force modulation amplitude, as illustrated in Fig. 4. Compared with previous work [48,49], it is notable that the leading-order potential is now linear in A since in these references it was reported to be quadratic. This is because past work only considered the case where the orbits were horizontal, $\theta_1 = \theta_2 = 0$; in that case, the leading order reported here vanishes, thereby leading to synchronization at order $O(A^2)$.

A limit that is easier to compare with previous work is when the vertical amplitude of motion, $R \sin \theta_i$, is assumed to be much smaller than the height h of the center of the orbit from the bottom wall. This assumption, that does not appear very relevant in the context of biology, is, however, what is usually done in the previous toy models [32,48]. Assuming $R \sin \theta_i \ll h$, we can then approximate $\langle y_1, y_2 \rangle \approx h^2/H^2$ and, after repeating the aforementioned procedure in the case of a single wall and in the case of the two walls, we

obtain

$$\begin{aligned}\frac{V_1(\Delta)}{\tilde{\beta}\Omega} &= \frac{A^2}{4}(1 - \cos \Delta)r_1(\pi - \theta_1, \theta_2) \\ &\quad \times \sin [2\delta - \Delta_0^{(1)}(\pi - \theta_1, \theta_2)], \\ \frac{V_2(\Delta)}{\beta\Omega} &= \frac{A^2}{4}(1 - \cos \Delta)r_2(\pi - \theta_1, \theta_2) \\ &\quad \times \sin [2\delta - \Delta_0^{(2)}(\pi - \theta_1, \theta_2)].\end{aligned}\quad (49)$$

where V_i is relevant for the case with i walls and r_i and $\Delta^{(i)}$ are the same as in the elastic compliance model but with the substitution $\theta_1 \mapsto \pi - \theta_1$. Again, $\tilde{\beta}$ is the same as previously defined above.

Just like the elastic compliance mechanism, force modulation therefore always leads to a single stable phase-locked state both for one and two walls. To examine the robustness of force modulation to strong hydrodynamic confinement, we examine in the next section the differences between the phase-locked states in two biologically relevant cases, and compare them to elastic compliance.

V. ROBUSTNESS OF SYNCHRONIZATION MECHANISMS

Since there are many degrees of freedom even in the minimal models we consider, it is difficult to compare the results obtained for different synchronization mechanisms across the entire parameter range. Furthermore, it is clear that some of the parameter values would be far from any of the biologically relevant limits that motivated this work originally. In this section, we therefore focus on two specific biological situations in order to set biologically relevant values for the parameters in our model.

Before introducing the details of the biological examples, we can already fix some of the model parameters by using the general knowledge of ciliary arrays. First, cilia are known to self-organize to all beat in the same direction [26,50]. Although hydrodynamic interactions could in theory play a role in setting this, it is a reasonable assumption that we will assume to be true in what follows. Using our notation, this means that $\alpha_1 = \alpha_2 = \alpha$. Secondly, the physical interpretation of the phase shift δ in the assumed force profile that we have used in our calculations, $F(\phi) = F_0[1 + A \sin(\phi + \delta)]$, is that the maximal drag on the cilium will occur when $\phi = \pi/2 - \delta$. Although it is rather difficult to measure this phase of maximal force, in the model that we are using here, $\phi = \pi/2$ represents the point at which the sphere is at its highest distance from the surface on which the cilium is attached. This means that at this phase the sphere is most exposed to the fluid drag and it is thus reasonable to assume that $\delta = 0$.

As demonstrated above, both physical mechanisms (elastic compliance vs force modulation) lead to stable phase-locked states. In order to quantify the difference in the synchronized states between the presence of two walls (strong confinement) and that of a single nearby surface, we then introduce the normalized distance μ_{1-2} between the ‘‘locked-in’’ phases on a unit circle, $\mu_{1-2} = (|\Delta_0^{(2)} - \Delta_0^{(1)}| \bmod \pi)/\pi$. Thus, $\mu_{1-2} = 0$ means that under both levels of confinement these locked-in phases are identical while if they differ by the maximal value of π the distance will take its maximal value of $\mu_{1-2} = 1$.

For the elastic compliance mechanism, the value of $\Delta_0^{(i)}$, with $i = 1, 2$ was previously defined as a stable fixed point of the phase difference. Similarly, in the context of force modulation, this definition extends to a stable fixed point obtained as a local minimum of $V(\Delta)$ inside the interval $[-\pi, \pi]$.

We now consider separately two common types of cilia, nodal and primary, due to their different geometrical features.

A. Nodal cilia

In this subsection, we first focus on the specific case of nodal cilia. These are found at the ventral surface of the node during the early stage of the embryo development. Nodal cilia are believed to cause the breaking of the left-right body symmetry by creating a leftward flow of the extraembryonic fluid [5]. The internal architecture of nodal cilia is slightly different than that of primary cilia. There is no central pair of microtubules, which makes nodal cilia beat in such a way that they trace a tilted conelike surface. The tilt of the orbit can be quite pronounced, as illustrated in Fig. 5 from mice experiments in Ref. [51]. The tilt in the mice embryos was measured to be $\theta = 40^\circ \pm 10^\circ$ in Ref. [47], while values in the range $\theta \in [15^\circ, 35^\circ]$ have also been reported in the literature [51]. Changing the mean tilt turns out to not affect our final results considerably, so, to capture the effect of the tilt variability on the synchronization, we assume $\theta_1 = 40^\circ$ and vary the value of θ_2 between 10° and 70° . It should be noted that our far-field model cannot describe the cases of nodal cilia that physically touch the epithelium cells (see the extensive tilt in Fig. 5) and thus the results that follow would not be applicable to such cases.

We consider two specific limits in which the results are compared. In one, we assume that the vertical extend of the orbit is much smaller than its height above the lower wall ($R \sin \theta_i \ll h$) while in the other, more realistic limit, we assume that those quantities are of similar magnitude, i.e., $R \sin \theta_i \lesssim h$. Note that, in the first case, the range of the tilt angle θ_i is still assumed to be that of nodal cilia (quoted above). This is meant to represent the small radius R limit, a limit that is not particularly biologically motivated but does stress the difference in the synchronization mechanisms, as shown below. The results of the elastic compliance mechanism are independent of the choice of the limit, but it makes a substantial difference in the results for the force modulation mechanism (see calculations in Sec. IV B).

Under the assumption $R \sin \theta_i \ll h$, we obtain that the force modulation mechanism leads to the same state of synchronization, with or without the upper wall, for any values of θ_1, θ_2 , and α . This can be seen from Eqs. (49) since both potentials have minimum at either 0 or π , with a stable point that depends only the sign of $\sin \Delta_0^{(1)}$ and $\sin \Delta_0^{(2)}$. From Eqs. (23) and (28), it is straightforward to see that these always have the same sign, as

$$\sin \Delta_0^{(1)} \sin \Delta_0^{(2)} = \frac{1}{2}r_1^{-1}r_2^{-1}(\cos \theta_2 - \cos \theta_1)^2 \sin^2 2\alpha \geq 0. \quad (50)$$

Consequently, the force modulation mechanism is absolutely robust to confinement and the synchronization dynamics is unchanged by the presence of the second nearby

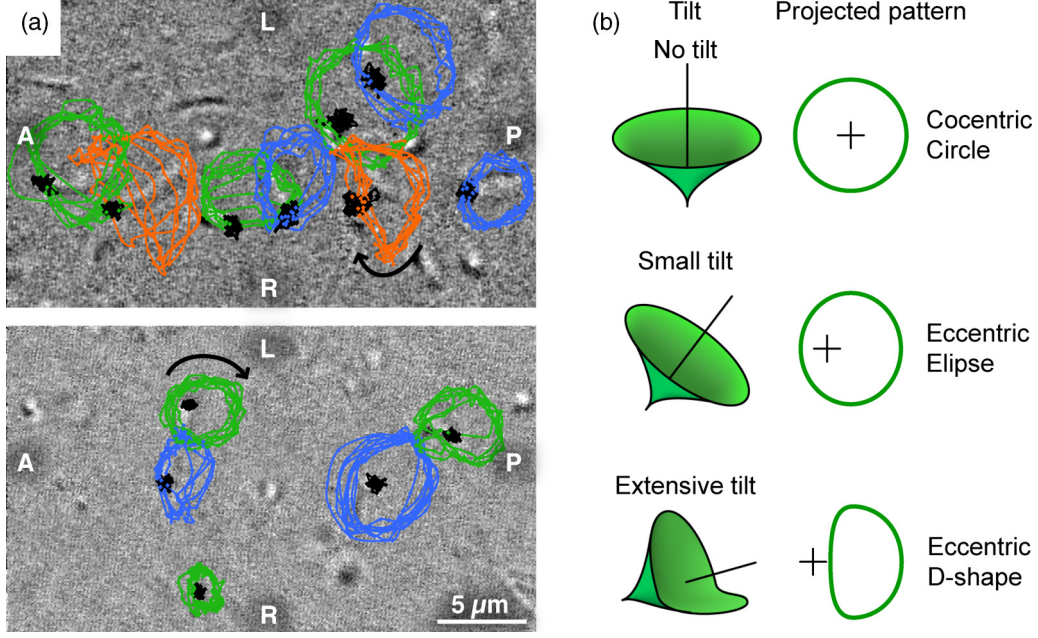


FIG. 5. Dynamics of nodal cilia in mice embryos. Experimental measurements of the trace of the cilium tip motion (left) are used to determine the average tilt of nodal cilia (right). Black dots indicate positions of the roots while the colored curves (blue, green and orange) show the trace of the tips of cilia. Blue and green traces indicate the small tilt in cilia (middle right) while the orange trace corresponds to the extensive tilt (bottom right). Reprinted with permission from Ref. [51], licensed under CC BY 4.0.

surface. In contrast, the elastic compliance mechanism does not provide the same level of robustness, as illustrated in Fig. 6(a) for fixed $\theta_1 = 40^\circ$. There, we see a plot of the measure μ_{1-2} , introduced above, for the elastic compliance mechanism. We fix the orbit of the first sphere to have the tilt $\theta_1 = 40^\circ$ equal to the average tilt of nodal cilia, and let the tilt of the second one vary between 10° and 70° . We also vary the angle $\alpha = \alpha_1 = \alpha_2$, which corresponds to the angle between the pumping direction and the vector connecting centres of the orbits. Warmer color in the plot indicates a higher value of μ_{1-2} and thus a lesser level of robustness. Visually, we can notice that for about a half of the $\{\alpha, \theta_2\}$ parameter space the elastic compliance mechanism leads to a similar synchronization state in both cases of confinement while for the other half of the space it leads to very different states. We will quantify this observation at the end of this section.

Under the different geometrical limit $R \sin \theta_i \lesssim h$, the coefficients in the potential from Eq. (37) become

$$C_0^{(2)} = -\frac{1}{2} \cos 2\alpha (\sin \theta_1 - \sin \theta_2), \quad (51)$$

$$B_1^{(2)} = -\frac{1}{8} \sin 2\alpha [-6 \sin(\theta_1 + \theta_2) + \sin 2\theta_1 + \sin 2\theta_2], \quad (52)$$

$$B_2^{(2)} = -\frac{1}{4} \sin 2\alpha [1 - \cos(\theta_1 - \theta_2)] \sin(\theta_1 + \theta_2), \quad (53)$$

$$A_1^{(2)} = -\frac{1}{4} (\sin \theta_1 - \sin \theta_2) \cos 2\alpha (\cos \theta_1 \cos \theta_2 - 3), \quad (54)$$

$$A_2^{(2)} = -\frac{1}{4} \cos 2\alpha (\sin \theta_1 - \sin \theta_2) (1 - \cos \theta_1 \cos \theta_2), \quad (55)$$

where the superscript (2) indicates the two-wall case. In case of a single wall, these coefficients reduce to

$$C_0^{(1)} = -\frac{1}{4} (1 + \cos 2\alpha) (\sin \theta_1 - \sin \theta_2), \quad (56)$$

$$B_1^{(1)} = -\frac{1}{16} \sin 2\alpha [-6 \sin(\theta_1 + \theta_2) + \sin 2\theta_2 + \sin 2\theta_1], \quad (57)$$

$$B_2^{(1)} = -\frac{1}{8} \sin 2\alpha (1 - \cos(\theta_1 - \theta_2)) \sin(\theta_1 + \theta_2), \quad (58)$$

$$A_1^{(1)} = -\frac{1}{8} (\sin \theta_1 - \sin \theta_2) [\cos 2\alpha (\cos \theta_1 \cos \theta_2 - 3) - 3 - \cos \theta_1 \cos \theta_2], \quad (59)$$

$$A_2^{(1)} = -\frac{1}{8} (\sin \theta_1 - \sin \theta_2) [\cos 2\alpha (1 - \cos \theta_1 \cos \theta_2) + 1 + \cos \theta_1 \cos \theta_2]. \quad (60)$$

Comparing the two results, we see that the normalized potentials satisfy

$$\hat{V}^{(1)} = \hat{V}^{(2)} - \frac{1}{8} (\sin \theta_1 - \sin \theta_2) (2\Delta - (3 + \cos \theta_1 \cos \theta_2) \sin \Delta + \frac{1}{2} (1 + \cos \theta_1 \cos \theta_2) \sin 2\Delta). \quad (61)$$

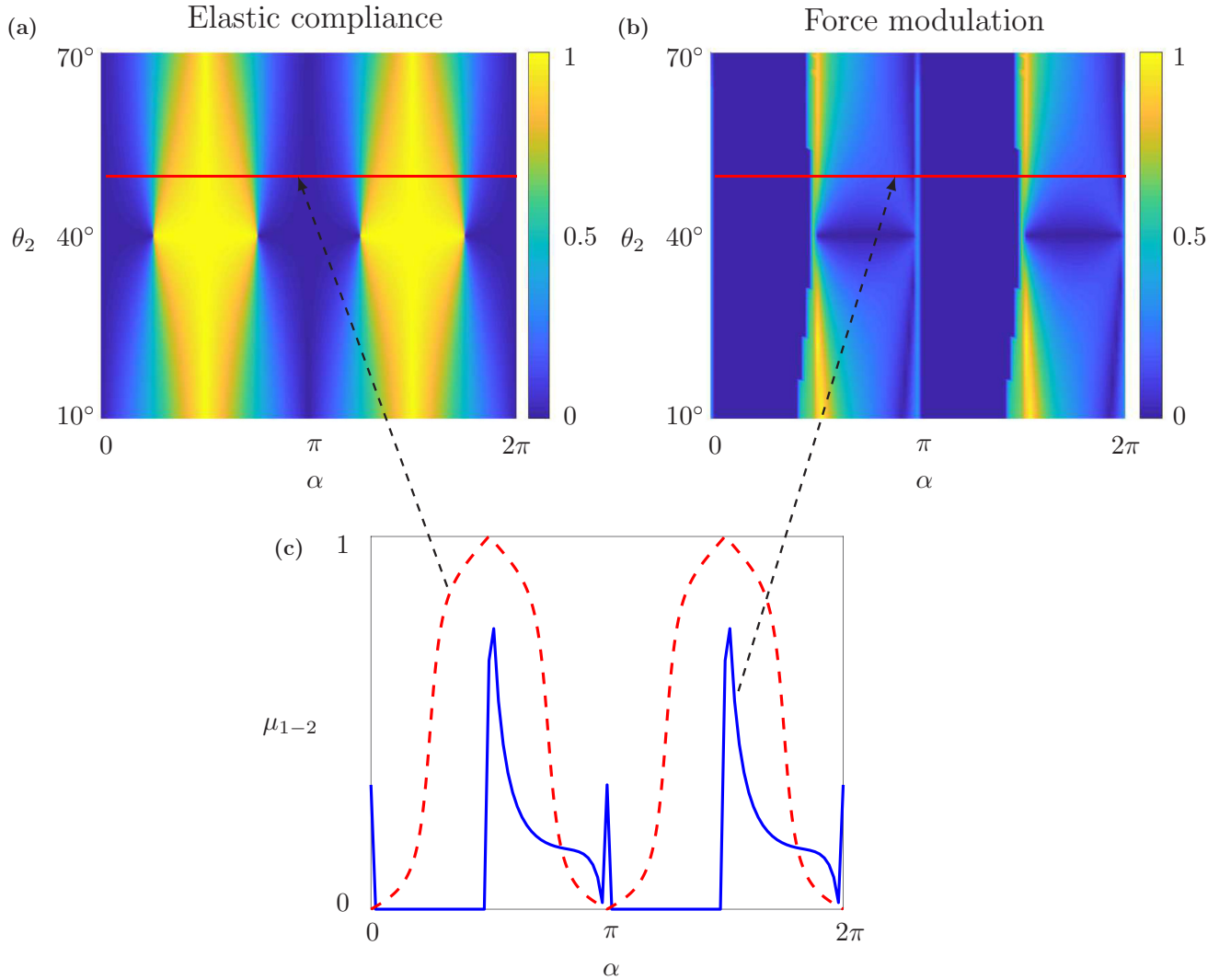


FIG. 6. Isovalues of the normalized phase difference, μ_{1-2} , comparing the stable phases to which the oscillators synchronize in cases of a single wall and two walls for the elastic compliance (a) and force modulation (b) mechanisms. Colors indicate the value of μ_{1-2} in the case $\alpha_1 = \alpha_2 = \alpha$ and $\theta_1 = 40^\circ$. The red line shows the location of the $\theta_2 = 50^\circ$ section shown in (c).

Bearing in mind that $\phi_1 - \phi_2 = \Phi_1 - \Phi_2 + O(A)$, we plot in Fig. 6(b) the values of the normalized difference in stable phases, μ_{1-2} , for the same choice and range of θ_i and α_i as was previously set for Fig. 6(a). As detailed above, results for the elastic compliance mechanism are independent of the choice of the geometric limit and hence Fig. 6(a) captures the robustness of this mechanism in the limit currently considered, as well. We first note that dependence on θ is much weaker than that on α . Secondly, it is clear from the figure that the force modulation mechanism [Fig. 6(b)] is significantly more robust to confinement than the elastic compliance mechanism [Fig. 6(a)]. This is further illustrated in Fig. 6(c) where we plot a section of the graphs for the specific value $\theta_2 = 50^\circ$.

To draw a quantitative conclusion on the robustness of the two mechanisms, we next introduce an integrated measure μ_I by relying on two assumptions drawn from known information on nodal cilia. First, we assume that the roots of cilia are isotropically distributed, i.e., that α is uniformly distributed in the interval $[0, 2\pi[$. Secondly, we choose the tilt θ_2 to be

normally distributed with mean 40° and standard deviation 10° , thus reflecting the experimental measurements from Ref. [47]. As a result, the integrated measure μ_I is defined as the integral

$$\mu_I = \frac{1}{2\pi C} \int_0^{2\pi} d\alpha \int_{10^\circ}^{70^\circ} d\theta_2 f_n(\theta_2) \mu_{1-2}(\alpha, \theta_2), \quad (62)$$

where $f_n(x) = (2\pi\sigma^2)^{1/2} \exp[-(x-m)^2/2\sigma^2]$, with $m = 40^\circ$, $\sigma = 10^\circ$, and $C = \int_{10^\circ}^{70^\circ} f_n(\theta_2) d\theta_2 \approx 0.9954$.

Using this definition, we can compute the values of μ_I for the two synchronization mechanisms. We obtain that for elastic compliance the value is $\mu_I^{EC} = 0.4871$, supporting the visual observation that for about a half of the parameter space the elastic compliance mechanism leads to a similar synchronization state in both cases of confinement (μ_{1-2} close to 0) while for the other half it leads to very different states (μ_{1-2} close to 1). In contrast, for the force modulation mechanism we obtain the much smaller value of $\mu_I^{FM} = 0.1178$,

TABLE I. Equations for the evolution of the phase difference for different levels of confinement (one vs two walls) and different synchronization mechanisms, i.e., elastic compliance (EC) vs force modulation mechanism (FM). Note that $B = [1 + 2(h - H)hR^{-2}] / 2$.

	One wall	Two walls
EC $\dot{\Delta} / \tau \omega^2 =$	$-\tilde{\beta} \cos^2 \alpha \sin \Delta$	$-\beta(y_1, y_2) \cos 2\alpha \sin \Delta$
FM $\langle \dot{\Delta} \rangle / \Omega A^2 =$	$-\frac{hR}{2H^2} \cos^2 \alpha (1 + 2 \cos \Delta) \sin \Delta$	$-\frac{R^3(2h-H)}{2H^4} \cos 2\alpha (\cos^2 \Delta + 2B \cos \Delta + B) \sin \Delta$

indicating a much higher level of robustness to confinement when compared to elastic compliance.

B. Primary cilia

In this second subsection, we investigate the robustness of the two synchronization mechanisms in the case of primary cilia. Unlike nodal cilia, primary cilia have a central pair of microtubules and additional internal structures that break the axial symmetry and guide these active filaments to beat in a plane perpendicular to the substrate to which they are attached. In terms of our model, this translates to assuming $\theta_1 = \theta_2 \approx \pi/2$, i.e., taking vertical orbits. We still keep the other assumptions outlined above and cilia beat in the same direction $\alpha_1 = \alpha_2 = \alpha$ with a maximal drag obtained at the highest point of the orbit, i.e., $\delta = 0$. Under these assumptions the equations for the evolution of the phase difference become simplified and are given in Table I.

We first note that both mechanisms in either case of confinement do exhibit stable fixed points of the phase difference, meaning that in all cases the system synchronizes to a fixed phase difference. For a single wall, both mechanisms lead to the in-phase synchronization for almost all pumping directions α (excluding when $\cos \alpha = 0$, which is a set of measure zero). On the other hand, in the case of two walls, the value of the ultimate phase difference depends not only on the mechanism but also on the sign of $\cos 2\alpha$. Specifically, the elastic compliance mechanism with two walls leads to in-phase synchronization if $\cos 2\alpha > 0$ but opposite phase ($\Delta = \pi$) if $\cos 2\alpha < 0$. The force modulation mechanism similarly leads to in-phase synchronization if $\cos 2\alpha > 0$ but if $\cos 2\alpha < 0$ the system synchronizes to a phase difference

whose value depends on the geometry of the orbit; it is given by $\Delta = \pm \Delta_0(h, R)$ with

$$\cos \Delta_0 = -\frac{1}{2} + \frac{h(H-h)}{R^2} - \left(\frac{h^2(H-h)^2}{R^4} - \frac{1}{4} \right)^{1/2}. \quad (63)$$

Interestingly, having in mind the geometrical limits $R < h$ and $R < H - h$ (i.e., the orbit has to fit between the walls), the range of possible values for this geometry dependent phase difference is relatively narrow, $1.94 < \Delta_0 < 2\pi/3 \approx 2.09$ (in radians), and thus the dependence on the nonorientational parameters of the orbit is weak.

Even though the mathematical results in the case of primary cilia are clearer than for the nodal cilia, the results for the robustness to synchronization are not as conclusive. In the geometric case $\cos 2\alpha > 0$, when cilia are pumping in a direction relatively close to the one joining their anchoring points (see illustrative summary in Fig. 7), both mechanisms lead to in-phase synchronization in both levels of confinement; we thus have perfect robustness to confinement in that case. In contrast, when $\cos 2\alpha < 0$, the elastic compliance mechanism leads to opposite-phase synchronization in the strongly confined setup so the robustness measure (see the start of the section) is $\mu_{1-2} = 1$. In the same situation, force modulation leads to a phase-locked state with a phase difference $\Delta_0 \approx 2\pi/3$ and thus a smaller robustness measure of $\mu_{1-2} \approx 2/3$. Unlike the nodal cilia case, it is therefore more difficult to definitely gauge the dominance of one mechanism over the other. Notably, this difference between the phase-locked states of the two cilia (π and $\Delta_0 \approx 2\pi/3$) obtained in half the parameter space (the domain where $\cos 2\alpha < 0$)

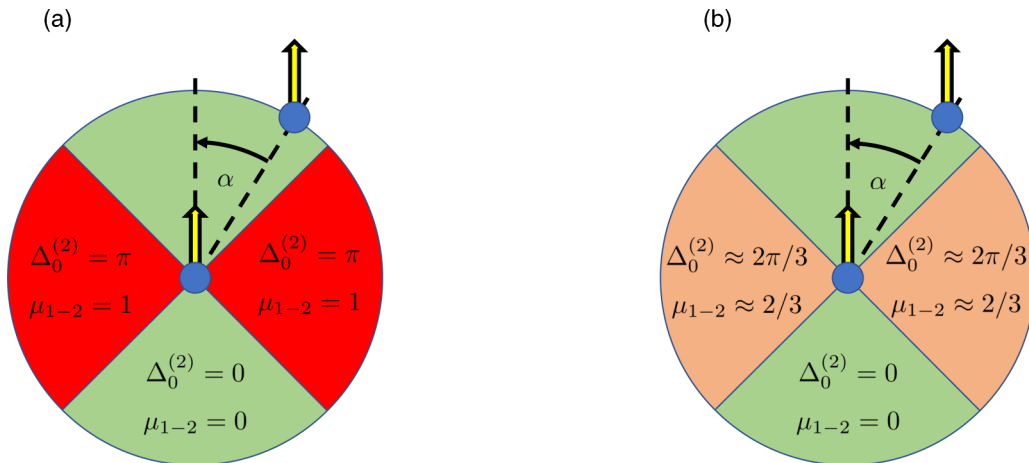


FIG. 7. Illustration of the dependence of the stable phase difference under strong confinement ($\Delta_0^{(2)}$) and the robustness measure (μ_{1-2}) on the relative position of two primary cilia. Results for the elastic compliance and force modulation mechanisms are shown separately in (a) and (b), respectively.

might be important in the collective organization of a large ciliary array.

VI. DISCUSSION

It is now well accepted that the synchronization of cilia is due to a combination of long-range hydrodynamic interactions with physical mechanisms allowing the ciliary phases to evolve. Two of such mechanisms have been identified by previous work, the elastic compliance of the periodic orbit or oscillations driven by phase-dependent biological forcing, both of which can lead generically to stable phase locking. In this paper, we used minimal models of cilia to theoretically investigate the effect of strong confinement on the effectiveness of hydrodynamic synchronization.

Specifically we have compared the usual ciliary dynamics near a single no-slip wall to the dynamics arising when a second nearby surface is introduced. We called this confinement strong because the distance between the surfaces is much smaller than the typical distance between the cilia. We computed separately the impact of hydrodynamic confinement on the synchronization dynamics of the elastic compliance and the force modulation mechanisms and compared our results to the standard case where the cilia are orbiting near a single surface. Applying first our results to the biologically relevant situation of nodal cilia rotating near surfaces, we show that force modulation is a mechanism with a higher chance,

than the elastic compliance mechanism, to lead to similar phase-locked states under strong confinement to those without confinement. Our results point therefore to the robustness of force modulation for synchronization of nodal cilia, an important feature for biological dynamics suggesting that it could be the physical mechanism most essential overall in these ciliary arrays. In the second biologically relevant situation of primary cilia, whose beat patterns are qualitatively different from those of nodal cilia, results on robustness are not as pronounced but still favor the force modulation mechanism.

Although, to the best of our knowledge, experiments have yet to investigate issues of synchronization under strong confinement, recent results using the algae of the genus *Chlamydomonas* confined in channels about twice their sizes have shown the important role of the higher moments of the distribution of viscous forces in the far-field flow of these motile cells [52]. Combined with these results, the modeling approach presented in our paper could be adapted to study flagellar synchronization in the case where the cells on which the flagella are anchored are free to move in the fluid.

ACKNOWLEDGMENTS

This project has received funding from the European Research Council under the European Union's Horizon 2020 Research and Innovation Programme (Grant No. 682754 to E.L.) and from Trinity College, Cambridge (IGS scholarship to I.T.).

-
- [1] C. Huygens, *Oeuvres complètes de Christiaan Huygens* (M. Nijhoff, Leiden, 1899), Vol. 8.
 - [2] H. A. Allard, The synchronal flashing of fireflies, *Science* **44**, 710 (1916).
 - [3] P. Laurent, The supposed synchronal flashing of fireflies, *Science* **45**, 44 (1917).
 - [4] R. Y. Moore, A clock for the ages, *Science* **284**, 2102 (1999).
 - [5] H. Hamada, C. Meno, D. Watanabe, and Y. Saijoh, Establishment of vertebrate left–right asymmetry, *Nat. Rev. Genet.* **3**, 103 (2002).
 - [6] R. E. Goldstein, M. Polin, and I. Tuval, Noise and Synchronization in Pairs of Beating Eukaryotic Flagella, *Phys. Rev. Lett.* **103**, 168103 (2009).
 - [7] H. C. Berg and R. A. Anderson, Bacteria swim by rotating their flagellar filaments, *Nature (London)* **245**, 380 (1973).
 - [8] H. Machemer, Ciliary activity and the origin of metachrony in paramecium: Effects of increased viscosity, *J. Exp. Biol.* **57**, 239 (1972).
 - [9] J. R. Blake and M. A. Sleight, Mechanics of ciliary locomotion, *Biol. Rev.* **49**, 85 (1974).
 - [10] D. R. Brumley, M. Polin, T. J. Pedley, and R. E. Goldstein, Metachronal waves in the flagellar beating of *Volvox* and their hydrodynamic origin, *J. R. Soc., Interface* **12**, 20141358 (2015).
 - [11] S. Gueron, K. Gurevich, N. Liron, and J. J. Blum, Cilia internal mechanism and metachronal coordination as the result of hydrodynamical coupling, *Proc. Natl. Acad. Sci. USA* **94**, 6001 (1997).
 - [12] F. Hayashi, Sperm co-operation in the fishfly, *Parachauliodes japonicus*, *Funct. Ecol.* **12**, 347 (1998).
 - [13] I. H. Riedel, K. Kruse, and J. Howard, A self-organized vortex array of hydrodynamically entrained sperm cells, *Science* **309**, 300 (2005).
 - [14] M. Polin, I. Tuval, K. Drescher, J. P. Gollub, and R. E. Goldstein, *Chlamydomonas* swims with two “gears” in a eukaryotic version of run-and-tumble locomotion, *Science* **325**, 487 (2009).
 - [15] D. R. Brumley, K. Y. Wan, M. Polin, and R. E. Goldstein, Flagellar synchronization through direct hydrodynamic interactions, *eLife* **3**, e02750 (2014).
 - [16] R. Di Leonardo, A. Búzás, L. Kelemen, G. Vizsnyiczai, L. Oroszi, and P. Ormos, Hydrodynamic Synchronization of Light Driven Microrotors, *Phys. Rev. Lett.* **109**, 034104 (2012).
 - [17] J. Kotar, M. Leoni, B. Bassetti, M. C. Lagomarsino, and P. Cicuta, Hydrodynamic synchronization of colloidal oscillators, *Proc. Natl. Acad. Sci. USA* **107**, 7669 (2010).
 - [18] B. Chakrabarti and D. Saintillan, Hydrodynamic Synchronization of Spontaneously Beating Filaments, *Phys. Rev. Lett.* **123**, 208101 (2019).
 - [19] G. I. Taylor, Analysis of the swimming of microscopic organisms, *Proc. R. Soc. London A* **209**, 447 (1951).
 - [20] K. Y. Wan and R. E. Goldstein, Coordinated beating of algal flagella is mediated by basal coupling, *Proc. Natl. Acad. Sci. USA* **113**, E2784 (2016).
 - [21] M. J. Kim and T. R. Powers, Hydrodynamic interactions between rotating helices, *Phys. Rev. E* **69**, 061910 (2004).
 - [22] S. Gueron and K. Levit-Gurevich, Energetic considerations of ciliary beating and the advantage of metachronal coordination, *Proc. Natl. Acad. Sci. USA* **96**, 12240 (1999).

- [23] J. G. Wakefield, C. A. Moores, and K. Wan, Coordination of eukaryotic cilia and flagella, *Essays Biochem.* **62**, 829 (2018).
- [24] R. Golestanian, J. M. Yeomans, and N. Uchida, Hydrodynamic synchronization at low Reynolds number, *Soft Matter* **7**, 3074 (2011).
- [25] S. Gueron and N. Liron, Simulations of three-dimensional ciliary beats and cilia interactions, *Biophys. J.* **65**, 499 (1993).
- [26] B. Guirao and J.-F. Joanny, Spontaneous creation of macroscopic flow and metachronal waves in an array of cilia, *Biophys. J.* **92**, 1900 (2007).
- [27] M. C. Lagomarsino, P. Jona, and B. Bassetti, Metachronal waves for deterministic switching two-state oscillators with hydrodynamic interaction, *Phys. Rev. E* **68**, 021908 (2003).
- [28] P. Lenz and A. Ryskin, Collective effects in ciliar arrays, *Phys. Biol.* **3**, 285 (2006).
- [29] A. Vilfan and F. Jülicher, Hydrodynamic Flow Patterns and Synchronization of Beating Cilia, *Phys. Rev. Lett.* **96**, 058102 (2006).
- [30] B. Qian, H. Jiang, D. A. Gagnon, K. S. Breuer, and T. R. Powers, Minimal model for synchronization induced by hydrodynamic interactions, *Phys. Rev. E* **80**, 061919 (2009).
- [31] M. Reichert and H. Stark, Synchronization of rotating helices by hydrodynamic interactions, *Eur. Phys. J. E* **17**, 493 (2005).
- [32] T. Niedermayer, B. Eckhardt, and P. Lenz, Synchronization, phase locking, and metachronal wave formation in ciliary chains, *Chaos* **18**, 037128 (2008).
- [33] N. Uchida and R. Golestanian, Generic Conditions for Hydrodynamic Synchronization, *Phys. Rev. Lett.* **106**, 058104 (2011).
- [34] B. Afzelius, Cilia-related diseases, *J. Pathol.* **204**, 470 (2004).
- [35] R. Lyons, E. Saridogan, and O. Djahanbakhch, The reproductive significance of human Fallopian tube cilia, *Hum. Reprod. Update* **12**, 363 (2006).
- [36] R. Faubel, C. Westendorf, E. Bodenschatz, and G. Eichele, Cilia-based flow network in the brain ventricles, *Science* **353**, 176 (2016).
- [37] T. Ishikawa and M. Hota, Interaction of two swimming paramecia, *J. Exp. Biol.* **209**, 4452 (2006).
- [38] J. Gray and G. J. Hancock, The propulsion of sea-urchin spermatozoa, *J. Exp. Biol.* **32**, 802 (1955).
- [39] G. T. Yates, How microorganisms move through water: The hydrodynamics of ciliary and flagellar propulsion reveal how microorganisms overcome the extreme effect of the viscosity of water, *Am. Sci.* **74**, 358 (1986).
- [40] C. Pozrikidis, The boundary integral equations, *Boundary Integral and Singularity Methods for Linearized Viscous Flow*, Cambridge Texts in Applied Mathematics (Cambridge University Press, Cambridge, 1992), pp. 19–75.
- [41] S. Camalet and F. Jülicher, Generic aspects of axonemal beating, *New J. Phys.* **2**, 24 (2000).
- [42] J. R. Blake, A note on the image system for a stokeslet in a no-slip boundary, *Math. Proc. Cambridge Philos. Soc.* **70**, 303 (1971).
- [43] N. Liron and S. Mochon, Stokes flow for a stokeslet between two parallel flat plates, *J. Eng. Math.* **10**, 287 (1976).
- [44] A. Pikovsky, M. Rosenblum, and J. Kurths, *Synchronization: A Universal Concept in Nonlinear Sciences*, Cambridge Nonlinear Science Series (Cambridge University Press, Cambridge, 2001).
- [45] H. Zhang, L. Koens, E. Lauga, A. Mourran, and M. Möller, A light-driven microgel rotor, *Small* **15**, 1903379 (2019).
- [46] D. R. Brumley, N. Bruot, J. Kotar, R. E. Goldstein, P. Cicutta, and M. Polin, Long-range interactions, wobbles, and phase defects in chains of model cilia, *Phys. Rev. Fluids* **1**, 081201(R) (2016).
- [47] J. Buceta, M. Ibañes, D. Rasskin-Gutman, Y. Okada, N. Hirokawa, and J. C. Izpisua-Belmonte, Nodal cilia dynamics and the specification of the left/right axis in early vertebrate embryo development, *Biophys. J.* **89**, 2199 (2005).
- [48] N. Uchida and R. Golestanian, Hydrodynamic synchronization between objects with cyclic rigid trajectories, *Eur. Phys. J. E* **35**, 135 (2012).
- [49] A. Maestro, N. Bruot, J. Kotar, N. Uchida, R. Golestanian, and P. Cicutta, Control of synchronization in models of hydrodynamically coupled motile cilia, *Commun. Phys.* **1**, 28 (2018).
- [50] H. Hagiwara, N. Ohwada, and K. Takata, Cell biology of normal and abnormal ciliogenesis in the ciliated epithelium, *Int. Rev. Cytol.* **234**, 101 (2004).
- [51] S. Nonaka, S. Yoshida, D. Watanabe, S. Ikeuchi, T. Goto, W. F. Marshall, and H. Hamada, De novo formation of left-right asymmetry by posterior tilt of nodal cilia, *PLoS Biol.* **3**, e268 (2005).
- [52] R. Jeanneret, D. O. Pushkin, and M. Polin, Confinement Enhances the Diversity of Microbial Flow Fields, *Phys. Rev. Lett.* **123**, 248102 (2019).